Arbitrary-order lensless ghost imaging with thermal light

Xi-Hao Chen[1], Ivan N. Agafonov[2], Kai-Hong Luo[1], Qian Liu[1], Rui Xian[1], Maria V. Chekhova[2], and Ling-An Wu[1]*
[1] *Laboratory of Optical Physics, Institute of Physics and Beijing National Laboratory for Condensed Matter Physics, Chinese Academy of Sciences, Beijing 100190, China*
[2] *Department of Physics, M. V. Lomonosov Moscow State University, Leninskie Gory, 119992 Moscow, Russia*

Arbitrary Nth-order ($N \geq 2$) lensless ghost imaging with thermal light has been performed for the first time by only recording the intensities in two optical paths. It is shown that the image visibility can be dramatically enhanced as the order N increases. It is also found that longer integration times are required for higher-order correlation measurements as N increases, due to the increased fluctuations of higher-order intensity correlation functions.

PACS numbers: 42.50.Dv, 42.25.Hz, 42.50.St

Compared with the first "ghost" imaging experiment with two-photon entangled light [1], second-order ghost imaging and ghost interference with thermal light [2, 3, 4, 5, 6, 7, 8, 9, 10, 11] has a low visibility which theoretically can never exceed 1/3, and in fact will be much lower than 1/3 in practical applications. Moreover, when a 2-dimensional high resolution image of a complex object is required, the better the resolution, the worse will its visibility be. This is one of the limitations for the practical application of thermal ghost imaging (GI). Fortunately, recent studies [12, 13, 14, 15, 17, 18] on the higher-order intensity correlation effects of thermal light show that the visibility can be significantly improved by increasing the order N. In this way, the drawback of low visibility in correlated imaging with thermal light can be overcome.

Third-order GI with thermal light has been theoretically analyzed to a certain extent [12, 19], but recently Liu *et al* pointed out that it is inappropriate to assume that second-order correlations play the entire or dominant role [13]. In their investigations of higher-order thermal ghost imaging and interference Liu *et al* showed that it is N-photon bunching that characterizes the Nth-order correlation and leads to the high-visibility in Nth-order schemes. The necessary condition for achieving a ghost image or interference pattern in Nth-order intensity correlation measurements is the synchronous detection of the same light field by different reference detectors. Multi-photon interference experiments have been carried out by Agafonov *et al* [14], verifying the conclusion that the visibility limits of three-photon and four-photon interference are respectively 82% and 94% for classical coherent light, as predicted theoretically by Richter [15]. Cao *et al* discussed N-th order intensity correlation in double-slit ghost interference with thermal light and proposed a scheme to study the visibility and resolution of the fringes with two detectors [17]. However, in their actual experiment only one CCD detector was employed, and the measurements were taken first with and then without the double-slit in place. Similar high-order schemes to obtain higher visibility but for GI were also suggested by Agafonov *et al* a little earlier [18].

In this paper we report the first demonstration of an arbitrarily high Nth-order lensless GI experiment with pseudothermal radiation. We do not actually need N light paths but measure the Nth-order intensity correlations by means of just two detectors. Moreover, when certain conditions are met, no lens is required for obtaining a well-focused image of the object.

Generally, in an Nth-order intensity correlation measurement, the light beam needs to be divided into N parts, each of which passes through an optical system and then is registered by a detector. In the high-intensity limit, the normalized Nth-order intensity correlation function is given by [17, 21]

$$g^N(x_1, ..., x_N) = \frac{\langle I_1(x_1)...I_N(x_N)\rangle}{\langle I_1(x_1)\rangle ... \langle I_N(x_N)\rangle}, \qquad (1)$$

where $I_j(x_j)$ is the instantaneous intensity at position x_j in the transverse direction, and $\langle ...\rangle$ stands for ensemble averaging, in practice achieved through time averaging. It is well known that $g^N(x) = \langle I^N(x)\rangle / \langle I(x)\rangle^N = N!$ for polarized thermal light when all the points in Eq. 1 are the same space-time point [21, 22]. This N-th order intensity correlation function g^N can thus be obtained by measuring the autocorrelation function of $I(x)$, as has been done in the 2nd order GI and interference-diffraction experiments with pseudothermal light [3, 16, 17], with mere knowledge of the intensity distribution $I(x)$ of that space-time point. It is thus reasonable to envisage a setup in which we have n beams of one intensity distribution (say passing through an object) and $N - n$ beams of another distribution (as reference arms), so that the instantaneous intensities $I_1(x_1) = I_2(x_2) = ... = I_n(x_n) = I(y_1)$ and $I_{n+1}(x_{n+1}) = I_{n+2}(x_{n+2}) = ... = I_{N-n}(x_{N-n}) = I(y_2)$. Then the transverse normalized Nth-order correlation function may be defined as

$$g_n^{(N)}(y_1, y_2) = \frac{\langle I^n(y_1) I^{N-n}(y_2)\rangle}{\langle I(y_1)\rangle^n \langle I(y_2)\rangle^{N-n}}, \qquad (2)$$

where the intensity correlation is composed of an n-fold

*Corresponding author: wula@aphy.iphy.ac.cn

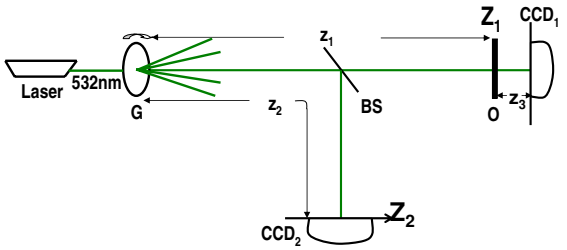

FIG. 1: (Color online) Experimental setup for arbitrary-order lensless GI with a pseudothermal light source. G: rotating ground glass plate; BS: beamsplitter; O: object.

intensity product at position y_1 and an $(N-n)$-fold product at position y_2, so there are $N-1$ ways to measure the Nth-order correlation function [13, 17]. This equation implies that, in GI, an arbitrary order correlation function can be obtained with mere knowledge of the two intensity distributions $I(y_1)$ and $I(y_2)$.

Here we consider a simple experimental scheme such as that shown in Fig. 1, which is basically the same as that for lensless 2nd-order correlation ghost imaging [11]. To pass to higher-order intensity correlation measurements, the signals of the test and reference detectors must be raised to the powers n and $N-n$. It should be mentioned that the correlation function measured this way is not the same as that in an N-port HBT interferometer, but the difference vanishes in the high-intensity limit as classical intensity fluctuations (excess noise) become stronger than quantum fluctuations. We consider the intensity distributions $I(y_1)$ and $I(y_2)$ of the speckle fields on the Z_1 and Z_2 planes located, respectively, at distances z_1 and z_2 from the thermal source. For simplicity but without loss of generality, in the derivation below the image is considered to be one-dimensional in the Z_1 plane.

If $T(y)$ indicates the field transmission function of the object, and a bucket detector is used in the test (object) arm, the bucket signal S is

$$S = \int I(y_1)\,|T(y_1)|^2 dy_1. \tag{3}$$

If we assume uniform illumination so that $\langle I(y_1)\rangle = I$, the average value of S is

$$\langle S\rangle = I\int |T(y_1)|^2\, dy_1 = IA_{obj}, \tag{4}$$

in which A_{obj} is equal to the object area when $|T(y_1)|^2$ is a step function equal to 1 inside the object and 0 outside. In the classical limit we can also write the Nth-order correlation function for GI as

$$\gamma_n^{(N)}(y_2) \;=\; \frac{\left\langle S^n I^{N-n}(y_2)\right\rangle}{\langle S\rangle^n \left\langle I(y_2)\right\rangle^{N-n}} \tag{5}$$

where we have assumed that all the n test arms have the same configuration, i.e., contain the same objects in the same positions and identical bucket detectors. It is evident that this requirement can be simply satisfied with a single test beam and the detector output divided into n parts. Since the same reasoning can be applied to the reference arms, we can thus perform any Nth-order correlation measurement with a simple experimental setup similar to that for 2nd-order lensless imaging in which only two light paths are needed, as shown in Fig. 1. The reference detector output is correspondingly divided into $N-n$ parts [23]. From the viewpoint of photodetection, the relation between the photocurrent $i(x,t)$ and light intensity $I(x,t)$ is [21] $i(x,t) \propto (1/T)\int_{-T/2}^{T/2} I(x,t+\tau)d\tau$, where T is the exposure time of the detector. If s and i are the photocurrents of CCD1 and CCD2, respectively, then from Eq. 5 the Nth-order correlation function for GI is

$$\gamma_n^{(N)}(y_2) \;=\; \frac{\left\langle (s/n)^n (i(y_2)/(N-n))^{N-n}\right\rangle}{\langle s/n\rangle^n \left\langle i(y_2)/(N-n)\right\rangle^{N-n}}. \tag{6}$$

This is the expression that is actually used in our data processing. The total intensity of the light source is assumed to be equal to the sum of the intensities of all the test and reference paths.

An outline of the experimental set-up is shown in Fig. 1. A CW laser beam with a wavelength λ of 532 nm and beam diameter D of 3 mm is projected onto a ground-glass plate G rotating at a speed of 0.7 rad/s to form pseudothermal light. The scattered beam is separated by a $50\%-50\%$ non-polarizing beamsplitter (BS) into two beams. The transmitted beam passes through the object, and the reflected beam is the reference beam. The two beams are detected by the charged-coupled-device (CCD) cameras CCD1 (Imaging Source DMK 21BU04) and CCD2 (Imaging Source DMK 31BU03), respectively. The object (a mask), which is the Chinese character for "light" shown in Fig. 2(a), is placed in the test arm where CCD1 plays the role of a bucket detector. The distance z_1 between the source and the object is equal to the distance between the source z_2 and CCD2, namely, z_1=z_2=240 mm. Thus the coherence area A at the plane Z_1 is about 16 μm^2, according to the well-known relationship of $A \sim (\lambda z_1/D)^2$; z_3 is the distance between the mask and CCD1 and is equal to 70 mm for the high-order imaging experiments. The cameras are operated in the trigger mode and are synchronized by the same trigger pulse. The data are acquired with an exposure time (0.1 ms) much shorter than the correlation time of the light source, which is on the order of 0.2 s, and saved through a USB cable to a computer.

Figures 2(b) and (c) show the images of the mask obtained by direct exposure on the camera CCD1 alone for z_3 = 20 mm and 70 mm (not in the bucket detection mode), after averaging over 20,000 frames. We see that Fig. 2(c) is a completely blurred image due to interference-diffraction effects, while Fig. 2(b) is quite a clear projected image since the CCD camera is close behind the mask.

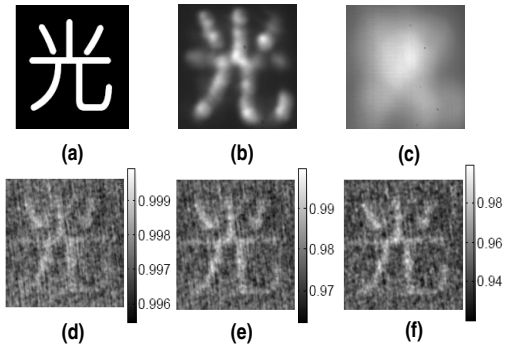

FIG. 2: First row: (a) Object mask. (b) and (c): Projection images obtained by CCD1 alone, averaged over 20,000 frames, for (b) $z_3 = 20$ mm and (c) $z_3 = 70$ mm. Second row: High-order ghost images obtained with thermal light in a lensless setup, averaged over 140,000 frames, corresponding to (d) 2nd order ($N = 2, n = 1$), (e) 10th order ($N = 10, n = 9$), (f) 20th order ($N = 20, n = 19$).

Though we cannot obtain a first-order image in the case of z_3 =70 mm, we can obtain clearly discernible higher-order ghost images ($N \geq 2$), as shown in the lower half of Fig. 2. For these shots a total of 140,000 frames was grabbed by each camera per plot at a rate of about 1.35 Hz. The arbitrary-order correlation images are calculated according to Eq. 6 by a Matlab program in which the total intensity s of each frame recorded by the bucket detector CCD1 is divided by n to give the intensity s/n of each component test arm, and similarly the output $i(y_2)$ of CCD2 which is captured at the same instant is divided by $N - n$ to give the intensity of each component reference beam; then the product of $(s/n)^n$ and $(i(y_2)/(N-n))^{N-n}$ is averaged over all the exposure shots and divided by $\langle s/n\rangle^n \langle i(y_2)/(N-n)\rangle^{N-n}$ to give the normalized Nth-order correlation function $\gamma_n^{(N)}(y_2)$. Here $\langle s\rangle$ and $\langle i(y_2)\rangle$ are obtained by averaging all the frames of CCD1 and CCD2, respectively. In our experiment $n = N - 1$ is chosen, as this gives the best visibility with the minimum number of frames to be processed. The reconstructed 2nd, 10th and 20th order ghost images which are normalized following $\gamma_n^{(N)}(y_2)/(\gamma_n^{(N)}(y_2))_{Max}$ are shown in Figs. 2(d), (e) and (f), respectively. It can be clearly seen that the image visibility increases with increasing N, as predicted. This is one of the chief advantages of GI systems. Another advantage is that the position distribution of the light intensity transmitted through the mask is not necessary in any-order GI, so long as all of the light is captured by the bucket detector. This has been demonstrated by Meyers *et al* who succeeded in obtaining 2nd-order ghost images even with a turbid distortive medium placed between the object and bucket detector [24].

It should be remarked that the rate of increase of the visibility in object imaging is much lower than that in interference experiments, such as the Nth-order Hanbury

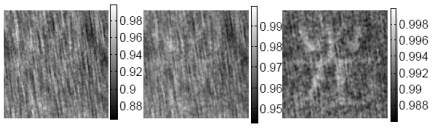

FIG. 3: 4th-order lensless ghost images for $n = 1, 2$, and 3 (from left to right).

Brown-Twiss and interference experiments reported by Cao *et al* [17]. This is because the number $M_{obj} = A_{obj}/A_{coh}$ of coherent areas falling inside the object, which is defined in Ref. [20], is very high and the visibility decreases with the increase of M_{obj}. Moreover, it should be noted that there is, in fact, a different number of coherent areas $M_{obj}^{(N)}$ within the object for each different order intensity correlation measurement if we define the coherent area (the resolvable area under the focused condition) as the square of the full-width-half-max $\delta y^{(N)}$ of the Nth-order intensity correlation function. For a given N, $M_{n,obj}^{(N)}$ is also different when n is different. It has been shown that the visibility increases with the order N when N is not very high, while it is independent of the resolution and close to unity at very high N [17, 18].

It should be pointed out that in Nth-order lensless GI there are at least $N - 1$ experimental configurations, since n may be different. We take the 4th-order as an example to show the difference between them. In Fig. 3 the 4th-order ghost images for $n = 1, 2$, and 3 are obtained by processing the same number of frames (i.e. using the same integration time) after the exposures with the CCD cameras. It is evident that the image is completely blurred in the case of $n = 1$ while a good image is obtained when $n = 3$. It is found that the higher the order N, the longer is the integration time required for a clear image to be obtained. Moreover, for a given N the lower the n, the longer is the integration time required. This can be inferred from Eq. 6 where we can see from the self-correlation intensity product $i^{N-n}(y_2)$ between the reference signals (or s^n for the test signals) that as n decreases (or $N - n$ increases), the fluctuations of the higher-order correlation functions will increase. Since the

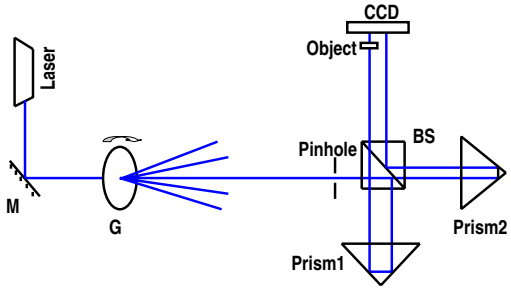

FIG. 4: (Color online) Experimental setup for arbitrary-order lensless GI with a pseudothermal light source. G: rotating ground glass plate; BS: beamsplitter; M: mirror.

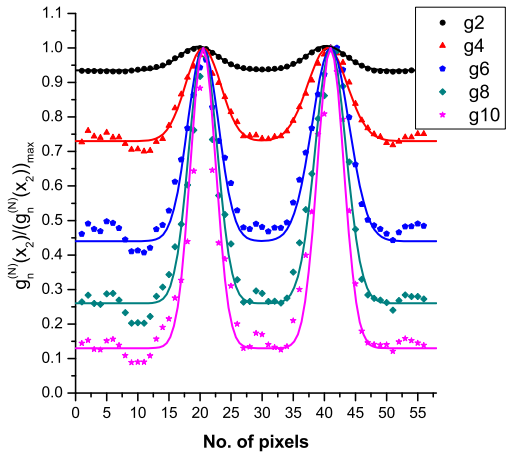

FIG. 5: (Color online) Experimental results of 2nd, 4th, 6th, 8th and 10th order lensless GI along one cross-section. Transverse coordinates are the number of pixels, and each point on the plot is an average of the raw data from 5 pixels. The solid lines are Gaussian fits.

fluctuation of the total intensity recorded by the bucket detector (the Nth-order self-correlation function of s) is less than the sum of the fluctuations of each pixel in the reference detector ($i(y_2)$), as we have indeed observed experimentally, it is best to choose a large n to obtain clearer images and save integration time.

We have also performed an experiment for a smaller M_{obj} using the experimental setup shown in Fig. 4. A He-Cd laser of wavelength 441.6 nm is reflected by a mirror (M) and used with a rotating ground glass plate (G) to form the pseudothermal light source, which is about 1 mm in diameter. A pinhole is placed 18 cm away from the ground-glass plate to limit the transverse size of the beam, which is separated by a $50\% - 50\%$ nonpolarizing beamsplitter (BS) into two beams. The reflected test beam is totally internally reflected by prism1, passes through BS and the object, and is detected on the lefthand side of a CCD camera (Imaging Source DMK 31BU03). The transmitted reference beam is reflected by prism2 and then by BS to be recorded on the righthand side of the detector. Both prisms can be translated to adjust the beam path distances between the light source and the detector. The object is a double-slit mask with slits of width 150 μm and separation 570 μm. As before, for lensless imaging the distances from the source to the object and reference detector are equal, z_1=z_2=354 mm. To make M_{obj} small enough, the data is only collected in one dimension along the transverse direction. The experimental results are shown in Fig. 5, in which $n = N/2$, and the 2nd, 4th, 6th, 8th and 10th order image cross-sections are obtained by averaging about 4,000 exposure frames. We can see that the image visibility increases much faster than in our previous experiment, mainly because here the number of features M_{obj} is much smaller.

In conclusion, we have reported the first demonstration of arbitrary-order ($N \geq 2$) lensless GI with pseudothermal light by only recording the intensities in two optical paths. The experimental results demonstrate that the image visibility can be dramatically enhanced as the order N increases. This overcomes the bottleneck of low visibility in 2nd-order ghost imaging with thermal radiation. It is conceivable that higher order GI could also be realized with a single detector setup using a laser and computer generated spatial modulation [25, 26], but for a real thermal light source the field distribution in the reference arm must be actually measured by at least one nonvirtual detector. As we have shown, in fact just one reference detector is sufficient. It is also found that longer integration times are needed as N increases, due to the increased fluctuations of higher-order intensity correlation functions. Moreover, for a given N the integration time increases with the decrease of n, so it is best to choose a large n to save time. The experimental setup for high-order GI is the same as that for the 2nd-order experiment, and we only require a program to calculate the image to any desired order of correlation. This makes GI with a thermal source even more promising than before for practical applications.

This work was supported by the National Natural Science Foundation of China (NNSFC Grants 60578029 and 10674174), the National Program for Basic Research in China (Grant 2006CB921107), the Russian Foundation for Basic Research (RFBR Grant 08-02-00555), and by a joint grant (RFBR 06-02-39015 GFEN) of RFBR and NNSFC.

[1] T. B. Pittman, Y. H. Shih, D. V. Strekalov, and A. V. Sergienko. Phys. Rev. A **52**, R3429 (1995).
[2] A. Gatti, E. Brambilla, M. Bache, and L. A. Lugiato, Phys. Rev. Lett. **93**, 093602 (2004).
[3] F. Ferri, D. Magatti, A. Gatti, M. Bache, E. Brambilla, and L. A. Lugiato. Phys. Rev. Lett. **94**, 183602 (2005).
[4] Y. J. Cai and S. Y. Zhu, Phys. Rev. E, **71**, 056607 (2005).
[5] D. Z. Cao, J. Xiong, and K. G. Wang, Phys. Rev. A **71**, 013801 (2005).
[6] A. Valencia, G. Scarcelli, Milena D'Angelo, and Y. Shih, Phys. Rev. Lett. **94**, 063601 (2005).
[7] Da Zhang, Yan-Hua Zhai, Ling-An Wu, and Xi-Hao Chen, Opt. Lett. **30**, 2354 (2005).
[8] Yan-Hua Zhai, Xi-Hao Chen, Da Zhang, and Ling-An Wu, Phys. Rev. A **72**, 043805 (2005).
[9] Yan-Hua Zhai, Xi-Hao Chen, and Ling-An Wu, Phys. Rev. A **74**, 053807 (2006).
[10] G. Scarcelli, V. Berardi and Y. H. Shih, Appl. Phys. Lett.

88, 061106 (2006); Phys. Rev. Lett. **96**, 063602 (2006).
[11] Xi-Hao Chen, Qian Liu, Kai-Hong Luo, and Ling-An Wu, Opt. Lett. **34**,695 (2009).
[12] Yanfeng Bai and Shensheng Han, Phys. Rev. A. **76**, 043828 (2007).
[13] Qian Liu, Xi-Hao Chen, Kai-Hong Luo, Wei Wu, and Ling-An Wu, Phys. Rev. A. **79**, 053844 (2009)
[14] I. N. Agafonov, M. V. Chekhova, T. Sh. Iskhakov, and A. N. Penin, Phys. Rev. A. **77**, 053801 (2008).
[15] T. Richter, Phys. Rev. A. **42**, 1817 (1990); Quant. Opt. **3**, 115 (1991).
[16] L. Basano and P. Ottonello, Opt. Exp. **15**, 12386 (2007).
[17] D. Z. Cao, J. Xiong, S. H. Zhang, L. F. Lin, L. Gao, and Kaige Wang, Appl. Phys. Lett. **92**, 201102 (2008).
[18] I. N. Agafonov, M. V. Chekhova, T. Sh. Iskhakov, and Ling-An Wu, J. Mod. Opt. **56**, 422 (2009).
[19] Li-Hua Ou and Le-Man Kuang, J. Phys. B. **40**, 1833 (2007).
[20] F. Ferri, D. Magatti, V. G. Sala, and A. Gatti, Appl. Phys. Lett. **92**, 261109 (2008).
[21] L. Mandel and E. Wolf, *Optical Coherence and Quantum Optics* (Cambridge University Press, 1995).
[22] R. Loudon, *The Quantum Theory of Light* (Oxford University Press,1983), Sec. 3.10.
[23] After our submission, a theoretical discussion of improved high-order visibility with a similar setup to ours was provided in: K. W. C. Chan, M. N. O'Sullivan, and R. W. Boyd, Opt. Lett. **34**, 3343 (2009).
[24] R. Meyers, K. S. Deacon, and Yanhua Shih, J. of Mod. Opt. **54**, 2381 (2007).
[25] J. H. Shapiro, Phys. Rev. A **78**, 061802(R) (2008).
[26] Y. Bromberg, O. Katz, and Y. Silberberg, Phys. Rev. A **79**, 053840 (2009).